Article

SOURCE DATA | TRANSPARENT PROCESS

THE EMBO JOURNAL

CPEB2-dependent translation of long 3′-UTR Ucp1 mRNA promotes thermogenesis in brown adipose tissue

Hui-Feng Chen, Chen-Ming Hsu & Yi-Shuian Huang*

Abstract

Expression of mitochondrial proton transporter uncoupling protein 1 (UCP1) in brown adipose tissue (BAT) is essential for mammalian thermogenesis. While human UCP1 mRNA exists in a long form only, alternative polyadenylation creates two different isoforms in mice with 10% of UCP1 mRNA found in the long form (Ucp1L) and ~90% in the short form (Ucp1S). We generated a mouse model expressing only Ucp1S and found that it showed impaired thermogenesis due to a 60% drop in UCP1 protein levels, suggesting that Ucp1L is more efficiently translated than Ucp1S. In addition, we found that β3 adrenergic receptor signaling promoted the translation of mouse Ucp1L and human Ucp1 in a manner dependent on cytoplasmic polyadenylation element binding protein 2 (CPEB2). CPEB2-knockout mice showed reduced UCP1 levels and impaired thermogenesis in BAT, which was rescued by ectopic expression of CPEB2. Hence, long 3′-UTR Ucp1 mRNA translation activated by CPEB2 is likely conserved and important in humans to produce UCP1 for thermogenesis.

Keywords alternative polyadenylation; brown adipose tissue; CPEB2; translational control; UCP1

Subject Categories Metabolism; Protein Biosynthesis & Quality Control; RNA Biology

DOI 10.15252/embj.201899071 | Received 23 January 2018 | Revised 13 August 2018 | Accepted 15 August 2018 | Published online 3 September 2018

The EMBO Journal (2018) 37: e99071

Introduction

Brown adipose tissue (BAT) is a central organ in thermogenesis. Uncoupling protein 1 (UCP1) in the inner mitochondrial membranes of BAT catalyzes a proton leak across the membrane to uncouple fuel oxidation from ATP synthesis and consequently generate heat (Cannon *et al*, 1998; Nedergaard *et al*, 2001; Chechi *et al*, 2013). Previous studies in mice with genetic ablation of BAT or UCP1 showed that UCP1-mediated BAT thermogenesis is important to manage body weight (Lowell *et al*, 1993; Kontani *et al*, 2005; Feldmann *et al*, 2009). The findings from fluorodeoxyglucose positron emission tomography (FDG-PET) imaging studies have demonstrated that BAT activity is correlated positively with resting metabolic rate but negatively with body mass index and percentage body fat in adult humans (van Marken Lichtenbelt *et al*, 2009). UCP1-dependent mitochondrial leak respiratory capacity in isolated supraclavicular BAT from people exposed to mild cold is ~1/3 of that in mouse interscapular BAT (Porter *et al*, 2016). Because humans and rodents have qualitatively similar UCP1 function, including uncoupling efficiency and sensitivity to GDP/ADP inhibition (Porter *et al*, 2016), the difference in total UCP1 activity per milligram BAT is likely due to the amount of UCP1 protein. Hence, inducing UCP1 expression to increase BAT thermogenesis has been proposed to combat obesity in humans (Dulloo, 2013).

Brown adipose tissue thermogenesis in response to nutrient or cold temperature (i.e., adaptive thermogenesis) is under the direct control of central sympathetic circuits to stimulate β3 adrenergic receptors (β3ARs; Lowell & Spiegelman, 2000; Dulloo, 2013; Morrison *et al*, 2014). Adrenergic-signaling upregulation of *Ucp1* transcription is important for adaptive thermogenesis, but the two posttranscriptional mechanisms identified to date inhibit UCP1 synthesis: insulin growth factor 2 mRNA-binding protein 2 (IMP2) suppressing *Ucp1* mRNA translation in BAT (Dai *et al*, 2015) and butyrate response factor 1 (BRF1) promoting *Ucp1* mRNA decay in high-fat diet (HFD)-challenged white fat (Takahashi *et al*, 2015). However, whether any posttranscriptional regulation exists to synergistically promote UCP1 synthesis with upregulated *Ucp1* transcription during adaptive thermogenesis remains unclear.

Two *Ucp1* mRNAs of different length in mice and rats were reported to encode the same UCP1 protein (Bouillaud *et al*, 1985), so the variable region is likely in the 3′-untranslated region (3′-UTR) and caused by alternative polyadenylation as shown in rabbit *Ucp1* (Balogh *et al*, 1989). The level of both *Ucp1* transcripts is increased in rodent BATs after cold exposure (Bouillaud *et al*, 1985; Puigserver *et al*, 1998), but no study has investigated their different contribution, if any, to thermogenesis. Only 10% of mouse *Ucp1* mRNA has a long 3′-UTR (*Ucp1L*), which is the only form for human *Ucp1*. The mouse model has been extensively used to understand the mechanisms controlling UCP1 synthesis, mammalian thermogenesis and the possible implications for human obesity, but the effect of differential *Ucp1* 3′-UTR processing on UCP1 expression

Institute of Biomedical Sciences, Academia Sinica, Taipei, Taiwan
*Corresponding author. Tel: +886 22652 3523; Fax: +886 22785 8594; E-mail: yishuian@ibms.sinica.edu.tw

has not been addressed. Such an effect could be significant because the regulatory sequences in the 3′-UTR often determine posttranscriptional efficiency of protein production (Moore, 2005; Barrett *et al*, 2012).

We found 2–3 cytoplasmic polyadenylation elements (CPEs) in both the human and mouse long *Ucp1* 3′-UTR, which are the consensus binding sites for the cytoplasmic polyadenylation element binding protein (CPEB) family of RNA-binding proteins, CPEB1–CPEB4. All CPEB proteins, with a similar carboxy-terminal RNA-binding domain (RBD) and a variable aminoterminal regulatory domain, can regulate target mRNA translation bidirectionally (Ivshina *et al*, 2014). CPEBs can function as a translational activator by enhancing polyadenylation of target mRNAs and consequently increasing translation initiation (Hagele *et al*, 2009; Igea & Mendez, 2010; Ortiz-Zapater *et al*, 2011; Pavlopoulos *et al*, 2011). When they function as a translational repressor, CPEB1 and CPEB4 inhibit translation at the initiation stage (Stebbins-Boaz *et al*, 1999; Hu *et al*, 2014), whereas CPEB2 downregulates translation at elongation (Chen & Huang, 2012).

In this study, we report that mouse and human *Ucp1* mRNAs differ in their 3′-UTRs. Using cultured mouse brown adipocytes and the *Ucp1ΔL* mouse model, we demonstrate more efficient translation of mouse *Ucp1L* than *Ucp1S* because *Ucp1L* mRNA underwent CPEB2-activated polyadenylation-enhanced translation in response to β3AR signaling. Mice lacking CPEB2 or *Ucp1L* mRNA showed reduced level of UCP1 protein and impaired thermogenesis. Ectopic expression of CPEB2 in CPEB2-knockout (CPEB2-KO) BAT restored UCP1-mediated thermogenesis. Our findings demonstrate that UCP1-mediated metabolic plasticity can be promoted at the post-transcriptional level, which is likely important in humans because they express only the long 3′-UTR *Ucp1* mRNA.

Results

Mouse and human *Ucp1* mRNAs differ in 3′-UTR and translation efficiency

A previous Northern blot study detected two *Ucp1* transcripts of different length in mouse BAT (Enerback *et al*, 1997) as did our study (Fig 1A). However, to our knowledge, no studies have examined the two isoforms separately when measuring the transcriptional change of *Ucp1*. Genetic mutations in *Ucp1* to disrupt its thermogenic function occur in multiple mammalian species (Gaudry *et al*, 2017), so we wondered whether the two transcripts contribute equally to UCP1 production. The deposited mouse *Ucp1* 3′-UTR sequence (NM_009463) contains two polyadenylation signals (AAUAAA), so we speculated that alternative polyadenylation may generate *Ucp1* mRNA with short and long 3′-UTRs, hereafter called *Ucp1S* and *Ucp1L*. Using the radiolabeled probe against the open reading frame (probe #1) or the unique 3′-UTR of *Ucp1L* (probe #2), we confirmed that the two *Ucp1* transcripts vary in their 3′-UTRs. The RNA-binding proteins IMP2 and BRF1 posttranscriptionally downregulate UCP1 synthesis to restrict thermogenesis (Dai *et al*, 2015; Takahashi *et al*, 2015). Unexpectedly, most of the *Ucp1* transcripts in mouse BAT (~90%) were *Ucp1S*, which contain no binding sequences for either IMP2 or BRF1. The BRF1-binding site in the *Ucp1* 3′-UTR (Fig 1A, UAUUUAU marked by a gray box) was experimentally identified (Takahashi *et al*, 2015). Although the previous study did not describe the IMP2-binding sites in *Ucp1* (Dai *et al*, 2015), UV-crosslinking and immunoprecipitation of IMP2 from cultured cells revealed its two primary binding motifs (AYAYA and YA_2YA, Y: pyrimidine; Conway *et al*, 2016), which were found in *Ucp1L* but not *Ucp1S* 3′-UTR (Fig 1A, underlined sequences). Moreover, two consensus cytoplasmic polyadenylation elements (CPEs, $UUUUA_{1\text{-}2}U$), which could be bound by CPEBs to promote polyadenylation-induced translation (Hake & Richter, 1994; Hagele *et al*, 2009; Ortiz-Zapater *et al*, 2011; Pavlopoulos *et al*, 2011; Ivshina *et al*, 2014), are present in only *Ucp1L* (Fig 1A).

The presence of very abundant *Ucp1S* mRNA with likely no 3′-UTR regulatory element in mice raises the question of which kind of *Ucp1* transcript is expressed in human BAT. We found only one deposited human *Ucp1* cDNA (ENST00000262999) with the 3′-UTR information; the *Ucp1* contains three CPEs but only one poly(A) signal (Fig 1B), so humans likely express only the *Ucp1L* form. No signal was detected by Northern blot analysis with 5 μg total RNA from human BAT samples (histology data in Fig EV1A), so we designed an RT–PCR strategy to allow for simultaneous amplification of *Ucp1L* and *Ucp1S* (Fig EV1B). Mouse BAT expressed both isoforms, which were absent in UCP1-KO BAT. In contrast, only the *Ucp1L* form was amplified from five human BAT samples (Fig 1B). Because of similar UCP1 activity in mouse and cold-stressed human BAT (~threefold less in humans; Porter *et al*, 2016) and *Ucp1* mRNA level much lower in our human BAT samples than mouse BAT (i.e., detectable *Ucp1* signal on Northern blot analysis with 1 μg mouse BAT total RNA), we surmised that the *Ucp1* transcript carrying the long 3′-UTR might be translated more efficiently. We performed a reporter assay with firefly luciferase (Fluc) appended with human *Ucp1* or mouse *Ucp1S* and *Ucp1L* 3′-UTR in brown adipocytes differentiated from HIB1B cells (Ross *et al*, 1992) and found that translation efficiency of Fluc reporter carrying long 3′-UTR from human and mouse was indeed threefold higher than that of short 3′-UTR (Fig 1C).

Conversion of *Ucp1L* to *Ucp1S* in mice decreases UCP1 synthesis and thermogenesis

To further prove that *Ucp1L*, contributing to only ~10% of total *Ucp1* mRNA, is translated more efficiently than *Ucp1S in vivo*, we used the CRISPR/Cas9 gene targeting strategy (Fig 2A) to generate *Ucp1ΔL* mice with *Ucp1* transcribed to only the short form (Fig 2B). The RT–PCR fragments amplified from *Ucp1S* were gel-isolated and sequenced to confirm that *Ucp1S* was processed identically in wild-type (WT) and *Ucp1ΔL* BAT (the end of *Ucp1S* sequence denoted by the arrowhead in Fig 1A). After crossing C57BL/6 mice for four generations, we used two independent lines (#30 and #64) and found UCP1 protein level reduced by more than 60% in *Ucp1ΔL* BAT from both mouse lines (Fig 2C), so data obtained from both lines were analyzed together. To monitor BAT temperature and its change during adaptive thermogenesis in ambulatory mice, we implanted a temperature probe onto the interscapular BAT pad (Gerhart-Hines *et al*, 2013; Lateef *et al*, 2014) and evoked adrenergic signaling by intraperitoneal injection of the β3AR agonist CL316243. Deficiency of *Ucp1L* mRNA reduced BAT temperature (Fig 2D) and the maintenance of β3AR signaling-induced thermogenesis (Fig 2E and Appendix Fig S1A). In contrast to upregulated

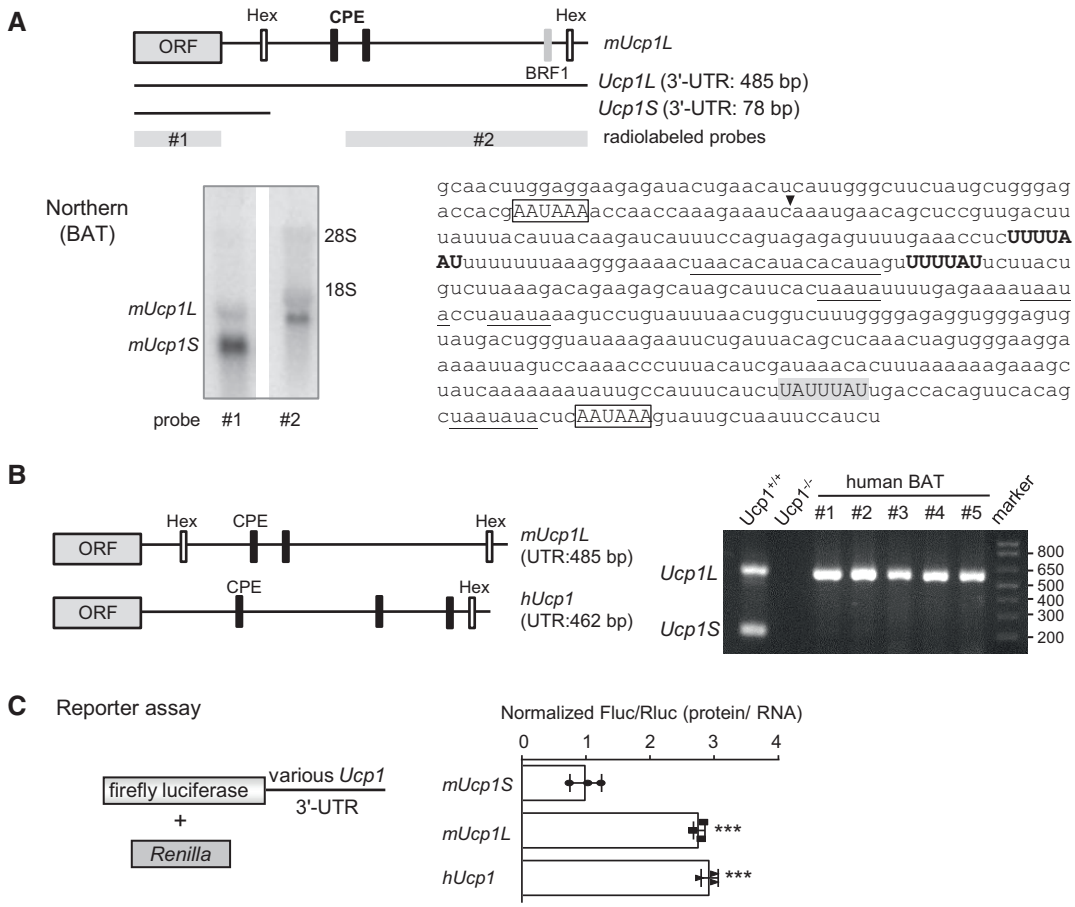

Figure 1. Alternative polyadenylation of mouse but not human *Ucp1* mRNA generates 3′-UTRs with different translation efficiency.

A The 3′-UTR sequence of m*Ucp1* RNA. Canonical CPEs ($UUUUA_{1\text{-}2}U$ in bold), the reported BRF1-binding site (UAUUUAU, gray box) and predicted IMP2-binding motifs (AYAYA and YA_2YA, underlined) are denoted. *Ucp1L* and *Ucp1S* carrying long and short 3′-UTRs, respectively, are resulted from alternative use of two polyadenylation signals (Hex: AAUAAA, open box). ORF, open reading frame. The arrowhead marks the end of *Ucp1S* sequence. Northern blots of *Ucp1* using 5 μg BAT total RNA and the denoted radiolabeled probes.

B Schematic comparison of *mUcp1L* and *hUcp1*. Poly(A) signal (Hex, open box) and CPE (black box) are denoted. The RT–PCR results from human, WT ($Ucp1^{+/+}$), and UCP1-KO ($Ucp1^{-/-}$) BAT RNA samples.

C Dual luciferase reporter assay and RT–qPCR. The reporter plasmids, Fluc-*mUcp1S*, Fluc-*mUcp1L*, or Fluc-*hUcp1L* 3′-UTR, and Rluc were co-transfected into differentiated HIB1B adipocytes. The transfected cells were used for luciferase activity assay and RT–qPCR. Data are mean ± SD from three independent experiments. Translation efficiency was defined as normalized activity (Fluc/Rluc) divided by normalized RNA level (*Fluc/Rluc*). ***$P < 0.001$ compared with Fluc-*mUcp1S*; one-way ANOVA.

expression of *Ucp2* mRNA in UCP1-KO BAT (Enerback *et al*, 1997), *Ucp1*, *Ucp2*, and *Ucp3* mRNA levels remained unchanged in BAT (Appendix Fig S1B), so the small amount of *Ucp1L* mRNA contributed to more than a half of the thermogenic ability of the mouse BAT. Impaired thermogenesis also resulted in increased BAT lipid content in the *Ucp1ΔL* BAT (Fig 2F).

CPEB2 activates polyadenylation-induced translation of *Ucp1L* mRNA

Mouse *Ucp1L* and human *Ucp1* contain two to three consensus CPEs (Fig 1B), which could be bound by CPEB family proteins to activate polyadenylation-induced translation (Hagele *et al*, 2009; Ortiz-Zapater *et al*, 2011; Pavlopoulos *et al*, 2011; Ivshina *et al*, 2014). Hence, we first determined which CPEB is expressed in BAT and thus may regulate *Fluc-Ucp1L* translation in HIB1B adipocytes (Fig 1C) by absolute quantitative PCR (qPCR) to estimate the mRNA levels of *Cpeb1*, *Cpeb2*, *Cpeb3*, and *Cpeb4*. All four *Cpeb* mRNAs were expressed to a comparable level of no more than threefold difference in BAT and HIB1B adipocytes (Fig EV2A). Therefore, we used the *Fluc-Ucp1L* reporter assay with the expression of individual myc-tagged CPEB or enhanced green fluorescent protein (EGFP) as a negative control in HIB1B adipocytes. Only CPEB2 stimulated the expression of *Fluc-Ucp1L* at the protein but not RNA level (Fig 2G). By using BAT isolated from CPEB2, CPEB3, and CPEB4 WT and KO male littermates (Chao *et al*, 2013; Tsai *et al*, 2013; Lai *et al*, 2016), we confirmed that only CPEB2 deficiency diminished UCP1 protein level (Fig 2H).

Nuclear localization of CPEB1 regulates alternative splicing (Lin *et al*, 2010; Bava *et al*, 2013) and alternative polyadenylation events

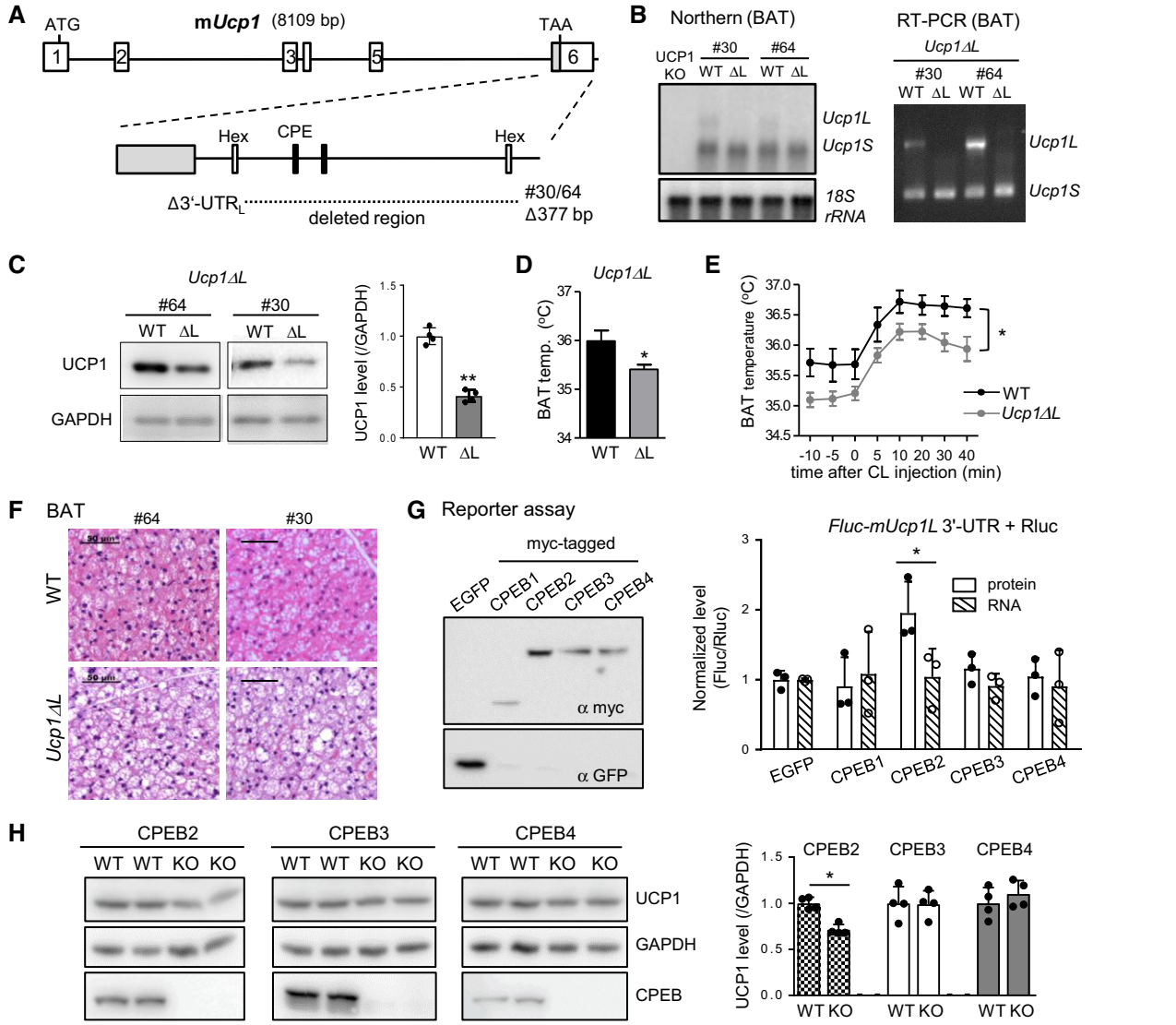

Figure 2. Reduced UCP1 protein level, BAT temperature and adrenergic signaling-induced thermogenesis in *Ucp1ΔL* mice.

A Two *Ucp1ΔL* mouse lines (#30 and #64) with a denoted deletion in the exon 6 of *mUcp1* gene.

B Northern blotting of *Ucp1 and 18S* rRNA and RT–PCR of *Ucp1L* and *Ucp1S* using total RNAs from the denoted BAT samples (two mice per genotype, 2 to 3 months old). The short PCR fragments were isolated for sequencing.

C Western blot analysis using WT and *Ucp1ΔL* BAT lysates. The protein level of UCP1 was normalized to GAPDH (4 months old, $n = 4$ per group). $^{**}P < 0.01$; Student's *t*-test.

D BAT temperature of WT ($n = 5$) and *Ucp1ΔL* ($n = 6$) male mice measured during 12-h light time. $^{*}P < 0.05$; Student's *t*-test.

E BAT temperature of WT ($n = 5$) and *Ucp1ΔL* ($n = 6$) male mice measured before and after i.p. injection of CL316243. $^{*}P < 0.05$; repeated-measures two-way ANOVA.

F Hematoxylin and eosin sections of BAT from 5-month-old WT and *Ucp1ΔL* male mice. Scale bars, 50 μm.

G Dual luciferase reporter assay. The reporter plasmids, Fluc-*mUcp1L* 3′-UTR, and Rluc were co-transfected with the plasmid expressing EGFP, or myc-tagged CPEB (immunoblots shown at the left) into differentiated HIB1B adipocytes (data from three independent experiments). $^{*}P < 0.05$ compared with EGFP; one-way ANOVA.

H Western blot analysis using BAT lysates prepared from various CPEB-WT and KO male littermates (4 months old, $n = 4$ per group). $^{*}P < 0.05$; Student's *t*-test.

Data information: Data are mean ± SEM in (D, E) and mean ± SD in (C, G, H).

(Bava *et al*, 2013). Although CPEB2, CPEB3, and CPEB4, mostly present in cytoplasm, have not been reported to control posttranscriptional RNA processing, blocking CRM1-mediated export results in their nuclear accumulation (Kan *et al*, 2010; Peng *et al*, 2010; Chao *et al*, 2012). Hence, all four CPEBs are able to shuttle between nucleocytoplasmic compartments. Nevertheless, CPEB2-KO and cold-induced adaptive thermogenesis did not change the ratio of *Ucp1S* to *Ucp1L* (Fig 3A), similar to CPEB3-KO and CPEB4-KO (Fig EV2B). To further examine whether CPEB2 directly binds to and promotes polyadenylation-induced translation of *Ucp1L* mRNA via β3AR signaling, BAT was harvested at 10 min after intraperitoneal injection of phosphate-buffered saline (PBS) or CL316243

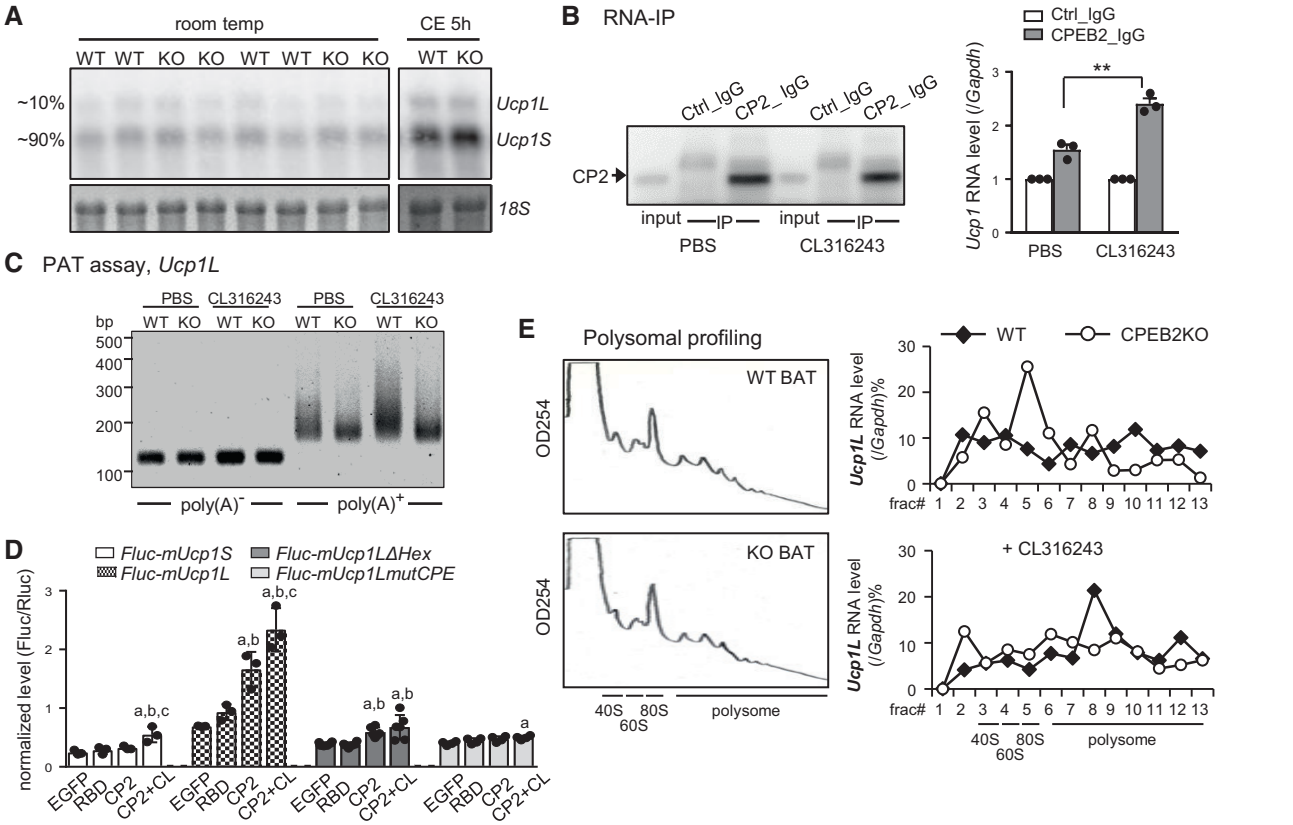

Figure 3. Adrenergic signaling enhances CPEB2-promoted polyadenylation and translation of *Ucp1L* RNA.

A Northern blotting of *Ucp1L* and *Ucp1S* in BAT from CPEB2-WT and -KO male mice at room temperature or after 5-h cold exposure (CE) at 4°C (five mice per genotype, 4- to 7-month-old).

B RNA immunoprecipitation (RNA-IP). BAT isolated from mice at 10 min after intraperitoneal (i.p.) injection of PBS or CL316243 was used for IP with control (Ctrl) or CPEB2 (CP2) IgGs. RT–qPCR analysis of precipitated substances for level of *Ucp1* mRNA with the non-target control, *Gapdh* RNA, as the reference. Data are mean ± SD (3- to 4-month-old male mice, $n = 3$ per group). $^{**}P < 0.01$; Student's *t*-test.

C PAT assay to monitor the poly(A) tail length of *Ucp1L* RNA in BAT isolated from 4-month-old WT and KO mice at 10 min after i.p. injection of PBS or CL316243. As a poly(A)$^-$ control, the oligo(dT)-annealed total RNAs were treated with RNaseH to remove poly(A) tails before PAT assay.

D Dual luciferase reporter assay. The reporter plasmids, Fluc-*mUcp1S*, Fluc-*mUcp1L*, Fluc-*mUcp1LΔHex*, or Fluc-*mUcp1LmutCPE* (the two CPEs were mutated to UUUUGGC and UUUGCC) 3′-UTR, and Rluc were co-transfected with the plasmid expressing EGFP, or myc-tagged full-length (CP2) or RNA-binding domain (RBD) of CPEB2 into differentiated HIB1B adipocytes. Cells were treated ± CL-316243 (CL) before harvesting for luciferase assay. Data are mean ± SD from three independent experiments. $^aP < 0.05$ compared with EGFP, $^bP < 0.05$ compared with RBD, and $^cP < 0.05$ compared with CP2; one-way ANOVA.

E Representative polysome profiles from CPEB2-WT and CPEB2-KO BAT. RT–qPCR analysis of the polysomal distribution of *Ucp1L* mRNA with RNA isolated from each fraction.

into CPEB2-WT and CPEB2-KO mice for RNA immunoprecipitation and PCR-based poly(A) tail (PAT) assay. The amount of *Ucp1L* mRNA in the precipitated substances was greater with CPEB2 IgG than control IgG (Fig 3B). Moreover, activation of β3ARs enhanced the binding of CPEB2 to *Ucp1L* mRNA (Fig 3B) and elongated the poly(A) tail length of *Ucp1L* mRNA, which was greatly impaired in CPEB2-KO BAT (Fig 3C). In contrast, the poly(A) length of *Ucp1S* mRNA was not affected by CPEB2 deficiency or β3AR signaling (Appendix Fig S2). The reporter assay in differentiated HIB1B adipocytes showed that only the full-length (CP2) but not the C-terminal RNA-binding domain (RBD) of CPEB2 or EGFP promoted the translation of *Fluc-mUcp1L*, which could be further potentiated by CL316243 treatment (Fig 3D). Such a CPEB2-enhanced translation was absent when using *Fluc-mUcp1S*, *Fluc-mUcp1LΔHex,* and *Fluc-mUcp1LmutCPE* reporters (Fig 3D), which suggests that CPEB2 promotes translation depending on the polyadenylation signal AAUAAA and CPEs. Moreover, CPEB2 deficiency did not affect global translation, as determined by polysome profiles (Fig 3E, left graphs), but it caused a shift of *Ucp1L* mRNA toward less dense sucrose fractions (i.e., a decrease in number of ribosomes associated with *Ucp1L*) with BAT ± CL316243 treatment (Fig 3E).

CPEB2-KO mice with reduced UCP1 expression have enlarged brown adipocytes

The loss of CPEB2 reduced UCP1 protein level in young (4-month-old, Fig 2H) and old (13-month-old, Fig 4A) male mice without changing *Ucp1* mRNA expression (Figs 3A and 4A). To assess whether CPEB2-upregulated UCP1 synthesis occurs in female mice, we examined the protein and mRNA levels of UCP1 in BAT from CPEB2-WT and CPEB2-KO female mice at different ages. Similar to KO male mice, KO female BAT at both young (4 months old) and

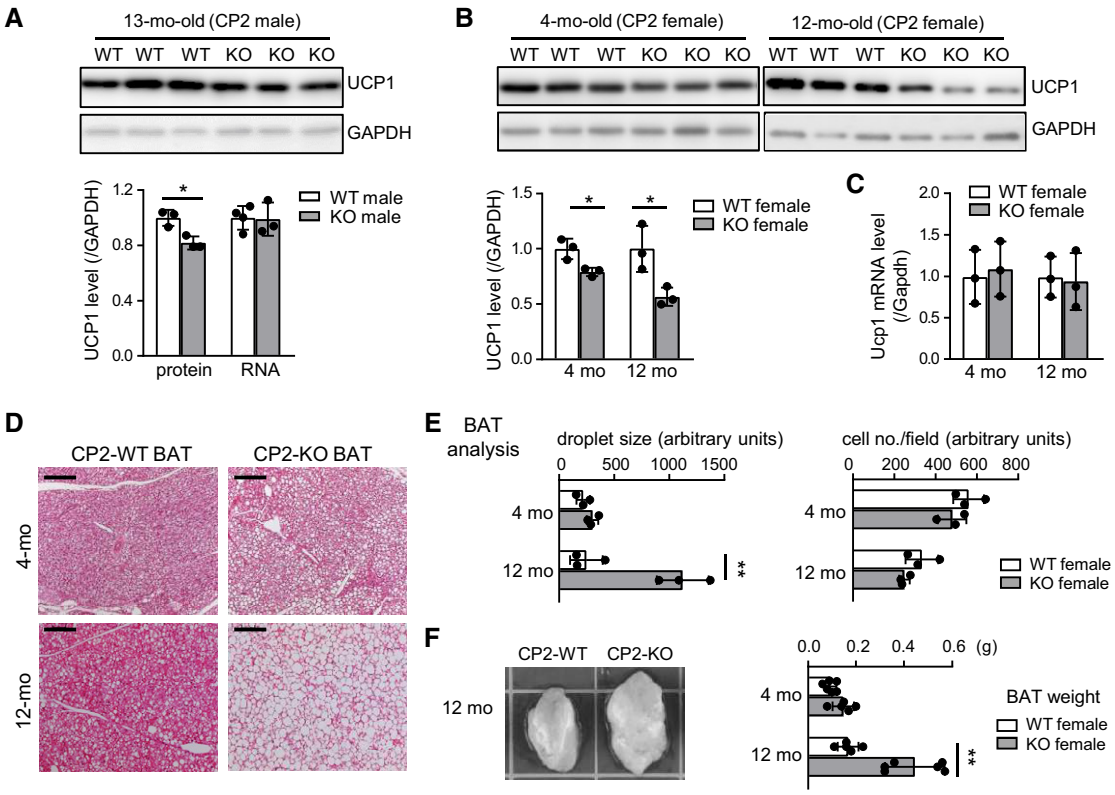

Figure 4. CPEB2-KO mice with decreased protein but not RNA level of UCP1 have enlarged brown adipocytes.

A Western blot analysis and RT–qPCR analysis of protein and mRNA levels of UCP1 and GAPDH in WT and KO male BAT (13 months old, n = 3–4 per group).

B Western blot analysis of UCP1 and GAPDH in BAT lysates from WT and KO female mice at 4 and 12 months old (n = 3 per group). Protein levels were normalized to that of GAPDH.

C RT–qPCR analysis of *Ucp1* mRNA level in BAT collected from (B) relative to *Gapdh* mRNA level.

D Hematoxylin and eosin sections of BAT from WT and CPEB2-KO female mice at 4 and 12 months old. Scale bars, 1 mm.

E Lipid droplet size and cell number (i.e., number of nuclei) in WT and KO BAT (representative images shown in 4D) were quantified and displayed as arbitrary units. Three tissue sections from each BAT and three mice per group were analyzed.

F Weight and representative images of WT and KO BAT. Three mice per group were analyzed.

Data information: All data are mean ± SD. *P < 0.05, **P < 0.01, Student's t-test.

old (12 months old) age showed decreased UCP1 protein level (Fig 4B) but not mRNA level (Fig 4C). Low thermogenic activity results in the accumulation of lipid droplets in brown adipocytes that was observed in UCP1-KO and bone morphogenetic protein 8b-KO mice (Kontani *et al*, 2005; Whittle *et al*, 2012). Indeed, CPEB2-KO female mice showed enlarged brown adipocytes as they aged (Fig 4D). In some mice, this change could occur as early as 4 months of age (one example in Fig 4D). Increased lipid droplet size but not cell number (Fig 4E) underlined the augmented BAT mass in CPEB2-KO mice (Fig 4F).

Decreased β3AR-potentiated energy expenditure and reduced metabolic activity in CPEB2-KO BAT

Reduced UCP1 level in CPEB2-KO and *Ucp1ΔL* BAT should cause inefficient non-shivering thermogenesis and a possible decrease in glucose utilization and metabolism, as indicated by deoxyglucose uptake in UCP1-KO mice (Inokuma *et al*, 2005) and rodents with altered thermogenic activity (Carter *et al*, 2011; Tomilov *et al*, 2014). Moreover, CPEB2 may regulate translation of other mRNAs besides *Ucp1* to affect BAT activity. Hence, we compared thermogenic and metabolic profiles between CPEB2-KO and *Ucp1ΔL* mice by using indirect calorimetry and PET imaging under ambulatory and anesthetized conditions, respectively.

The mice adapted to the metabolic cages were monitored for oxygen consumption and carbon dioxide production to calculate heat production according to the illustrated experimental design (Fig 5A). At temperatures below thermoneutrality (i.e., ~30°C for mice), the four groups of mice (CPEB2-KO, WT, *Ucp1ΔL,* and UCP1-KO) showed a temperature-dependent increase in energy expenditure (Fig 5B). Although CPEB2-KO, *Ucp1ΔL,* and UCP1-KO mice of both sexes tended to generate less heat than WT mice under 4°C exposure, only CPEB2-KO females and UCP1-KO mice of both sexes showed statistical differences (Fig 5B). Notably, female CPEB2-KO mice consistently showed reduced metabolic rates even at 30°C, which could not be attributed to UCP1-dependent thermogenesis (Fig 5B). Because other factors, such as housing temperature, ambulatory movement, and shivering

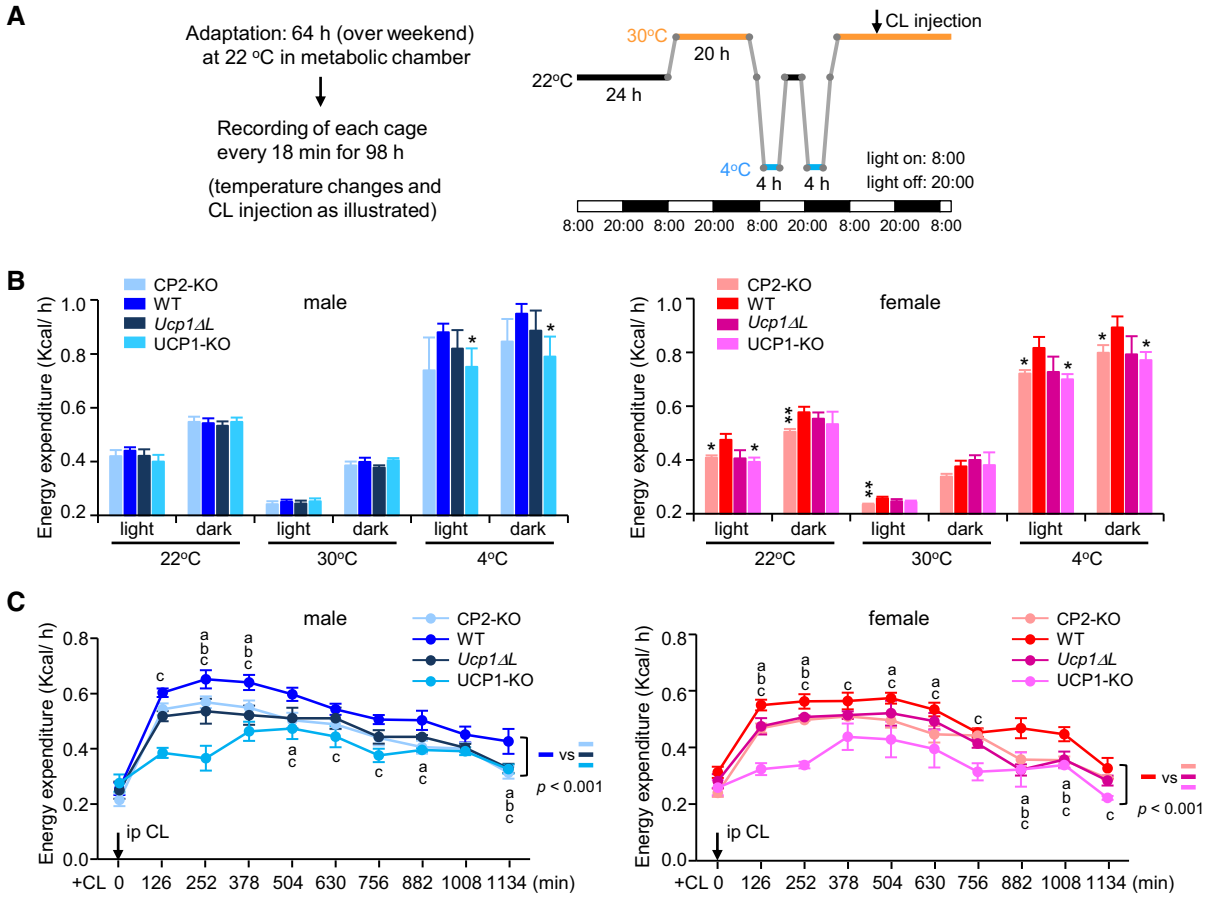

Figure 5. Altered energy metabolism in CPEB2-KO and *Ucp1ΔL* mice.

A Schematic designs for metabolic energy measurements at different temperatures and after i.p. injection of CL316243 (CL). Changes between two temperatures occurred linearly at 2 h.

B Average energy expenditure of 3.5- to 4.5-month-old male and female mice measured at 22, 30, and 4°C in Oxymax chambers under a light/dark period for 12, 10, and 4 h, respectively (CP2-KO/WT/*Ucp1ΔL*/UCP1-KO: n = 5/5/4/4 male mice and 5/6/5/3 female mice). WT mice were pooled from littermates of CP2-KO mice and *Ucp1ΔL* mice. *$P < 0.05$, **$P < 0.01$ compared with WT mice; one-tailed unpaired Student's t-test. All groups of mice showed similar mean body weight (CP2-KO/WT/*Ucp1ΔL*/UCP1-KO: male, 28.6 ± 1.6/33.4 ± 2.0/29.7 ± 2.6/30.4 ± 2.6 g; female, 26.4 ± 1.8/28.0 ± 1.8/27.6 ± 3.0/27.2 ± 3.0 g).

C Blunted CL-promoted energy expenditure in CP2-KO, *Ucp1ΔL*, and UCP1-KO mice of both sexes (***$P < 0.001$, compared with WT mice by two-way ANOVA). Data at the denoted time points are the average of seven data points acquired before a 126-min period. $^{a}P < 0.05$ CP2-KO mice, $^{b}P < 0.05$ *Ucp1ΔL* mice, or $^{c}P < 0.05$ UCP1-KO mice compared with WT mice by Tukey's *post hoc* test.

Data information: All data are mean ± SEM.

thermogenesis, confound the measurement of UCP1-dependent energy metabolism (Cannon & Nedergaard, 2011), we pharmacologically activated BAT at 30°C and monitored heat production in the four groups of mice. β3AR-evoked energy expenditure was significantly blunted in CPEB2-KO, *Ucp1ΔL*, and UCP1-KO mice of both sexes as compared with WT mice (Fig 5C, $P < 0.001$).

On PET imaging, which monitors metabolic rate by uptake of fluorodeoxyglucose (^{18}F-FDG), both female and male CPEB2-KO mice showed reduced metabolic activity of interscapular BAT at room temperature or after 5-h cold exposure but normal glucose consumption in the brain, liver, and whole body (Fig EV3A). However, ^{18}F-FDG uptake did not differ in *Ucp1ΔL* BAT of both sexes even after 5-h cold exposure (Fig EV3B). Thus, cold-activated adrenergic signaling appears to increase BAT ^{18}F-FDG uptake independent of UCP1 (Fig EV3B). Moreover, a significant decrease in ^{18}F-FDG uptake by CPEB2-KO BAT at both room temperature and after cold exposure is not simply caused by impaired UCP1 expression.

Ectopic BAT expression of CPEB2 in KO mice improves thermogenesis

Resting energy expenditure was diminished in female CPEB2-KO mice even under thermoneutrality (Fig 5B) and CPEB2-KO BAT was metabolically less active than *Ucp1ΔL* BAT (Fig EV3). Unlike the adipocyte-restricted pattern of UCP1, CPEB2 is expressed widely in various tissues (Lai *et al*, 2016). Thus, to clarify whether defective thermogenesis in CPEB2-KO mice, as indicated by β3AR-evoked energy expenditure (Fig 5C), is brown adipocyte-autonomous, we used a recombinant adeno-associated virus

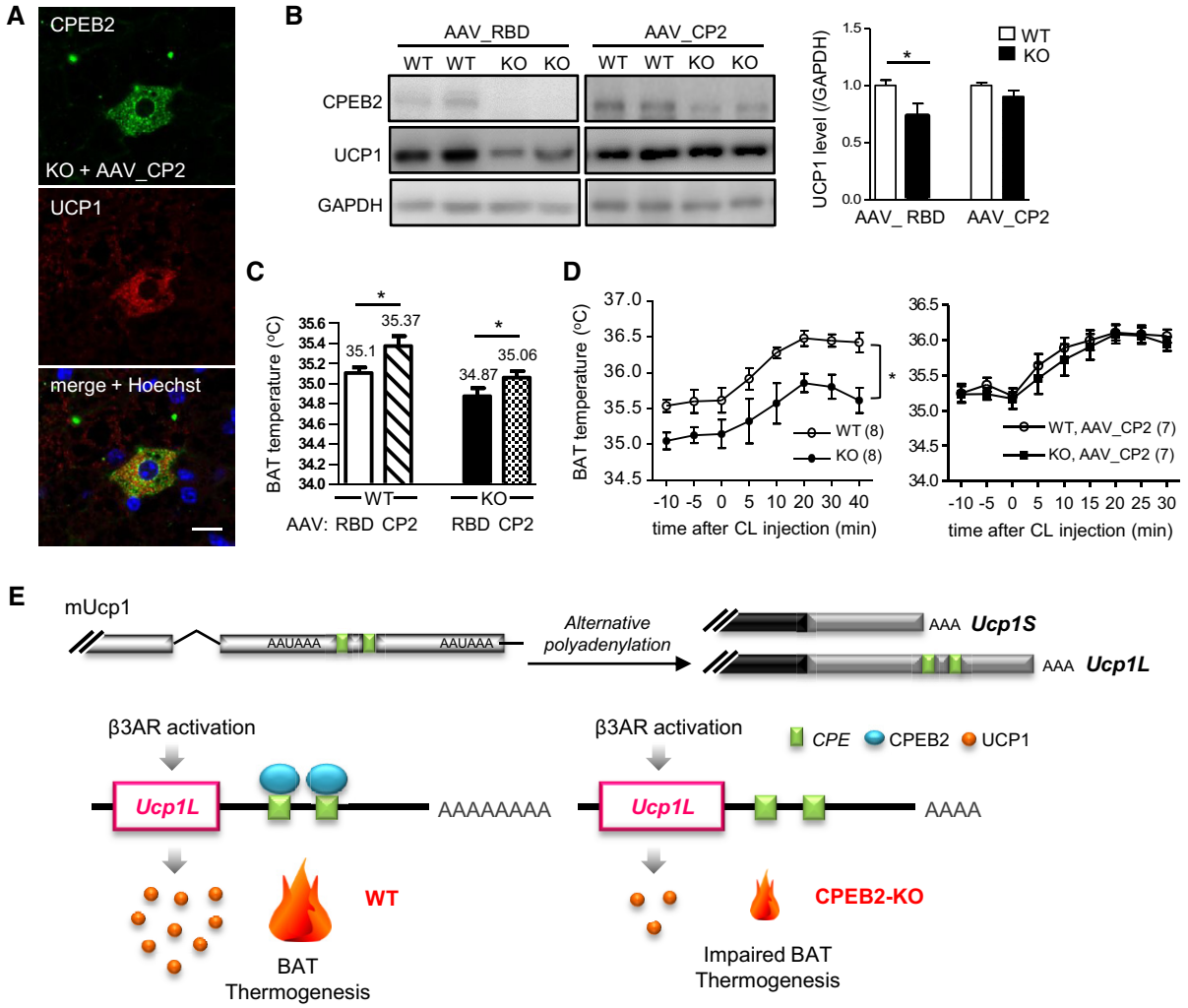

Figure 6. Ectopic expression of CPEB2 in the KO BAT increases UCP1 synthesis and improves thermogenesis.

A CPEB2-WT and CPEB2-KO mice were transduced with adeno-associated virus (AAV)-expressing full-length (AAV_CP2) or RNA-binding domain (AAV_RBD) of CPEB2. Immunostaining of CPEB2 and UCP1 in KO BAT transduced with AAV_CP2 for 2 weeks, with Hoechst staining of nuclei. Scale bar, 10 μm. See more images in Fig EV4D.

B Western blot analysis of UCP1 in BAT lysates from WT and KO male mice 2 weeks after AAV transduction (n = 6 mice per group). *$P < 0.05$; Student's t-test.

C BAT temperature of WT and KO male mice after 2 weeks of AAV transduction measured during 12-h light time (n = 7 mice per group). *$P < 0.05$; Student's t-test.

D BAT temperature in WT and KO male mice and of AAV_CP2-transduced WT and KO male mice (n = 7 mice per group) before and after i.p. injection of CL316243 (CL). *$P < 0.05$; repeated-measures two-way ANOVA.

E CPEB2 activates polyadenylation-induced translation of mouse *Ucp1* mRNA with long 3′-UTR via β3AR signaling for adaptive thermogenesis in BAT. Mice lacking the translational regulator CPEB2 show impaired BAT thermogenesis.

Data information: All data are mean ± SEM.
Source data are available online for this figure.

serotype 2/8 (AAV2/8) vector for packaging AAV because of its high targeting efficiency to adipose tissues when delivered intravenously (O'Neill *et al*, 2014). However, the virus was delivered directly into the KO BAT to restore CPEB2 level. We then addressed whether UCP1 expression and thermogenesis could be rescued. To estimate the AAV transduction efficiency, BAT injected with AAV-expressing EGFP was harvested 2 weeks later and stained with Hoechst to label nuclei. Approximately 50% of Hoechst-positive cells expressed EGFP after one 3-point injection (Figs EV4A and B). AAV-expressing full-length (AAV_CP2) or the RNA-binding domain (AAV_RBD) of CPEB2 was injected into the BAT of WT and KO mice. The RBD of CPEB2 binds to RNA but cannot activate translation (Fig 3D). Moreover, ectopic expression of RBD in WT BAT did not have a dominant negative effect on endogenous CPEB2 to compromise UCP1 expression (Fig EV4C), so it was used as a control to ensure that AAV infection itself did not affect UCP1 synthesis. Two weeks after AAV_CP2 transduction, increased UCP1-immunostained signal was observed in KO brown adipocytes expressing exogenous CP2 (Figs 6A and EV4D). Delivery of AAV_CP2 rescued the UCP1 expression in BAT of KO mice (Fig 6B) and improved their thermogenesis, as evidenced by 12-h mean BAT temperature (Fig 6C). Moreover, an increase in

BAT temperature evoked by the β3AR agonist CL316243 declined faster in KO than WT BAT (Fig 6D and Appendix Fig S3) and could be rescued by ectopic expression of CP2 (Fig 6D). In contrast, the early thermogenic response (i.e., within 20 min after CL316243 injection) appeared normal in CPEB2-KO mice (Fig 6D) and *Ucp1ΔL* mice (Fig 2E), which suggests that UCP1-mediated adaptive thermogenesis at this early stage is likely promoted by allosteric activators, such as free fatty acids generated from β3AR signaling-induced lipolysis (Rial & Gonzalez-Barroso, 2001; Liew *et al*, 2013; Liu *et al*, 2014) to potentiate its proton conductivity rather than increase its expression. The results from HIB1B adipocytes and the two mouse models, *Ucp1ΔL* and CPEB2-KO, have demonstrated that CPEB2-activated *Ucp1L* mRNA translation via β3AR signaling in BAT is critical to promote thermogenesis (Fig 6E).

Discussion

Ucp1 transcripts of different length were observed in rodents 30 years ago (Bouillaud *et al*, 1985; Balogh *et al*, 1989), but our results first demonstrate that differential 3′-end processing of *Ucp1* mRNA quantitatively affects UCP1 expression and thermogenesis in BAT. The loss of CPEB2-activated *Ucp1L* mRNA translation in BAT accounted for defective thermogenesis in CPEB2-KO and *Ucp1ΔL* mice. Such a β3AR signaling- and CPEB2-dependent translational response may be more important in humans, with their expression of only long 3′-UTR *Ucp1* mRNA.

Ucp1ΔL mice express less than ~60% of UCP1 in BAT (Fig 2C), so *Ucp1L* was estimated to translate with ~15-fold greater efficiency than *Ucp1S*. We speculate that the undetectable amount of *Ucp1* mRNA by Northern blotting in human BAT samples (Fig 1B) may be compensated by CPEB2-activated translation to produce sufficient UCP1. To compare the expression of *Ucp1* and *Cpeb2* mRNAs between mouse and human BAT, we used absolute qPCR quantification to estimate the amount of *Ucp1* and *Cpeb2* molecules in the cDNA samples. The expression of human *Ucp1* mRNA was only 1/30 to 1/300 the level in mice (Fig EV5A), but mouse and human *Cpeb2* mRNA levels were similar, with no relation between the levels of *Ucp1* and *Cpeb2* mRNA (Fig EV5A). The broad spectrum of *Ucp1* expression among the five individuals sampled is not likely caused by sampling variation because we detected no expression of Wilms tumor 1, a marker of white adipocyte progenitors, and no strong association with levels of two other brown adipocyte markers, early B-cell factor 2 and LIM homeobox protein 8 (Park *et al*, 2014; Wang & Seale, 2016; Fig EV5B).

By using a reporter assay, we confirmed that CPEB2 promoted the translation of *Fluc-hUcp1-3'UTR* in HIB1B adipocytes, which could be enhanced by CL316243 treatment (Fig EV5C). Moreover, two single nucleotide polymorphisms (SNPs) of low occurrence in the 3′-UTR of human *Ucp1*, SNP1 (rs538981371, [U/C]UUUAU), and SNP2 (rs940802197, UUUU[A/G]U); disrupted CPE; and downregulated CPEB2-activated *Fluc-hUcp1-3'UTR* translation (Fig EV5C). Thus, mouse *Ucp1L* translation activated by CPEB2, if fully functioning in human BAT, is estimated to generate the protein level to ~1/2 to 1/20 of that in mouse BAT. However, such a speculation remains to be validated because the human BAT tissues used for total RNA isolation (Fig EV1A) might not contain a pure population of brown adipocytes as mouse BAT.

β3AR signaling activates not only *Ucp1* transcription (Lowell & Spiegelman, 2000) but also CPEB2-mediated *Ucp1L* polyadenylation, which appears to increase translation rather than RNA stability because of no evident changes in *Ucp1L* mRNA levels in CPEB2-KO BATs (Fig 3A). Recent studies indicated that posttranscriptional regulation of *Ucp1* mRNA is related to HFD-induced obesity. IMP2 was found to downregulate the translation of *Ucp1* and several other mitochondrial protein mRNAs. IMP2-KO mice show reduced body weight, elevated mitochondrial number in several tissues, and increased UCP1 level in BAT (Dai *et al*, 2015). Nevertheless, cold exposure still induced UCP1 expression to a higher level in IMP2-KO than WT BAT, which cannot be simply explained by a translational de-repression mechanism in the absence of IMP2. Thus, IMP2 may affect UCP1 level by means other than translational repression. Perhaps the lack of IMP2 may favor CPEB2 binding to *Ucp1L* mRNA to promote translation because several predicted IMP2-binding motifs are in close proximity to CPEs (Fig 1A). Notably, activation of β3AR increased the association between CPEB2 and *Ucp1L* mRNA (Fig 3B) but whether such a change is caused by posttranslational modification of CPEB2 to enhance its RNA-binding ability or passively through the accessibility of CPEs, such as reduced IMP2 occupancy on *Ucp1L* mRNA, needs further investigation.

Knockout of Cnot7, a component of CCR4-NOT deadenylase complex, stabilized and increased *Ucp1* mRNA level by ~10-fold in inguinal white adipose tissue and by ~1.5-fold in BAT from mice with an HFD (32% fat), with no difference in UCP1 expression observed under a normal diet. Moreover, the binding of BRF1 to the UAUUUAU motif in *Ucp1* 3′-UTR (Fig 1A) is required to recruit the CCR4-NOT complex for *Ucp1* mRNA decay (Takahashi *et al*, 2015). Both studies used the Fluc reporter carrying the long *Ucp1* 3′-UTR to support the molecular actions (i.e., translational repression and RNA decay) of IMP2 in reticulocyte lysates and BRF1 in HEK293 cells, but they did not address the issue, given that the *Ucp1L* form contributes to only 10% *Ucp1* mRNA (Fig 1A). Moreover, if *Ucp1L* is the only form degraded by the CCR4-NOT complex and is expressed more abundantly than *Ucp1S* in BAT, we expected to observe a marked increase in *Ucp1S* level in *Ucp1ΔL* BAT, which was not the case (Fig 2B). Thus, the differential amount of *Ucp1L* and *Ucp1S*, at least in BAT, is likely determined by alternative polyadenylation instead of CCR4-NOT-mediated RNA decay.

Alternative polyadenylation, controlled by *cis*-elements located upstream and downstream of the polyadenylation signal (PAS, consensus AAUAAA or weak variants) in pre-mRNAs, could generate mRNAs carrying 3′-UTR of different lengths to modulate their stability and translation efficiency. The polyadenylation machinery in metazoans is composed of ~20 core proteins, including the multi-subunit cleavage and polyadenylation specificity factor (CPSF) complex (Tian & Manley, 2017). CPEB1 can bind to the CPSF160 subunit and recruit the CPSF complex on the PAS of target mRNAs to promote polyadenylation-induced translation in the cytoplasm (Mendez *et al*, 2000). Such an interaction in the nucleus also facilitates the CPSF complex recruitment to the nearby PAS (within ~100 bp upstream or downstream of CPE) of CPEB1-bound pre-mRNAs to control an alternative use of PAS (Bava *et al*, 2013). Although a PAS and a CPE at the proximal *Ucp1* 3′-UTR are close enough for possible

CPEB-mediated alternative polyadenylation (Fig 1A), deficiency of CPEB2, CPEB3, or CPEB4 did not affect PAS usage in *Ucp1* (Figs 3A and EV2B). Whether alternative polyadenylation of mouse *Ucp1* mRNA varies in different fat depots or with diet or cold climate stimulation and which RNA-binding proteins, such as CPEB1, IMP2, BRF1, or others, may regulate this event remain open questions.

^{18}FDG-PET imaging is widely used to indicate metabolic activity of organs and tumors *in vivo*. However, deoxyglucose with the 2-hydroxyl group of glucose substituted by hydrogen is taken by cells through glucose transporters and phosphorylated by hexokinase but unable to undergo further glycolysis. Thus, ^{18}FDG and ^{18}FDG-6-phosphate are trapped intracellular that can be detected by PET scanning. As such, ^{18}FDG-PET signal only reflects glucose uptake and hexokinase activity in tissues (Basu *et al*, 2014), so UCP1-mediated mitochondrial leak respiration acting downstream of glycolysis could not directly be monitored by ^{18}FDG-PET imaging. Although a previous study claimed that norepinephrine-stimulated uptake of 2-deoxy-^{3}H-glucose is impaired in UCP1-KO BAT (Inokuma *et al*, 2005), a recent report showed that UCP1-KO mice with reduced BAT temperature and oxygen consumption exhibited normal BAT uptake of ^{18}F-FDG in response to CL316243 treatment. Moreover, glycolytic flux and 2-deoxy-^{3}H-glucose uptake in isolated UCP1-KO brown adipocytes were not affected despite defective uncoupled respiration (Hankir *et al*, 2017). Adrenergic stimulation by CL316243 (Hankir *et al*, 2017) or by cold exposure (Fig EV3B) appears to increase BAT ^{18}F-FDG uptake independent of UCP1. The loss of CPEB2-promoted *Ucp1L* translation does not account for decreased ^{18}FDG uptake in CPEB2-KO BAT (Fig EV3A). Similarly, despite comparable thermogenic responses on pharmacological activation of β3ARs in *Ucp1ΔL* and CPEB2-KO mice (Fig 5C), only CPEB2-KO females exhibited blunted heat production at different temperatures (Fig 5B), indicating that CPEB2 must regulate other CPE-containing mRNAs to affect BAT metabolism. Because of respiratory stress-associated neonatal death, the number of CPEB2-KO animals after weaning was about 30% of the expected Mendelian inheritance (Lai *et al*, 2016). *Ucp1ΔL* mice showed normal resting energy metabolism (Fig 5B), so to further investigate other factors besides UCP1 that contributed to diminished energy expenditure in surviving CPEB2-KO female mice, we will use adipose-specific KO mice to bypass neonatal lethality and determine whether depletion of CPEB2 in BAT is sufficient to recapitulate metabolic phenotypes found in CPEB2-KO mice (Figs 5 and EV3).

Deficiency of UCP1-mediated thermogenesis only slightly decreased energy expenditure in UCP1-KO mice at 4°C (Fig 5B) because acute cold exposure triggers heat production mostly through shivering thermogenesis by muscle contractions (Golozoubova *et al*, 2001). By contrast, adrenergic signaling-elevated expression of UCP1 in BAT and beige adipocytes is required for a vast increase in non-shivering thermogenic capacity and endurance of cold-acclimatized rodents (Puigserver *et al*, 1998; Golozoubova *et al*, 2001, 2006; Cannon & Nedergaard, 2011). Our CPEB2-KO animal model strongly supports that regulated translation efficiency of *Ucp1* mRNA by CPEB2 in BAT plays a critical role in "upping" thermogenesis. Whether CPEB2-activated *Ucp1L* translation also plays a role to upregulate UCP1 level in beige adipocytes during cold- or diet-induced adaptive thermogenesis and whether CPEB2-controlled translation is important for weight management and metabolic fitness in mice require further investigation.

Materials and Methods

Animals and genotyping

This study was approved by Institutional Animal Care and Utilization Committee of Academia Sinica (protocol no. 12-03-338). UCP1-knockout mice (UCP1-KO; stock no. 003124) were purchased from the Jackson Laboratory (Enerback *et al*, 1997). The generation of CPEB2-KO, CPEB3-KO, and CPEB4-KO mice in a C57BL/6 genetic background was previously described (Chao *et al*, 2013; Tsai *et al*, 2013; Lai *et al*, 2016). To generate *Ucp1ΔL* mice by CRISPR/Cas9 gene targeting technology, two small guide RNAs (sgRNAs in Appendix Table S1) targeted to mouse *Ucp1* along with *in vitro*-transcribed Cas9 RNA (Addgene plasmid #48625) were microinjected into 0.5-day C57BL/6 embryos, which were then transferred into ICR surrogate female mice. The tail samples from transgenic litters were used for PCR genotyping and sequencing to obtain founder mice with designated deletion. Two independent founders were backcrossed with C57BL/6 mice for four generations to avoid possible off-target editing. C57BL/6 mice were housed with a 12-h light/dark cycle in a climate-controlled room (22–24°C) with *ad libitum* access to water and food (LabDiet 5058 with 21.6% of calories from 9% fat). The genotypes were determined by PCR of tail biopsies and the KAPA mouse genotyping kit (KAPA Biosystems) as previously described (Chao *et al*, 2013; Tsai *et al*, 2013; Lai *et al*, 2016). The primers used to genotype UCP1-KO and *Ucp1ΔL* are in Appendix Table S1. All WT and KO mice, including *Ucp1ΔL* mice, were littermates from heterozygous crosses and assigned parallel to experiments without specific criteria or randomization. Unless otherwise specified in the figure legends, 4- to 5-month-old WT and KO male or female littermates were used for the experiments. Moreover, CPEB2-KO mice and *Ucp1ΔL* mice used at the time of experiments showed similar mean body weight with their WT littermates.

Antibody information

To generate monoclonal CPEB2 antibody in mice, we used the recombinant protein produced in *Escherichia coli*, containing the N-terminal 236 amino acids of rat CPEB2 (JF973322). Affinity-purified polyclonal CPEB3 antibody (Huang *et al*, 2006) and monoclonal CPEB4 antibody (Tsai *et al*, 2013) were described previously. The other antibodies are in Appendix Table S2.

Tissue collection, histology, and CL316243 treatment

Mice were euthanized with isoflurane inhalation before tissue isolation. Isolated tissues were snap-frozen in liquid nitrogen and stored at −80°C. Histological staining with hematoxylin and eosin was performed by the Institutional Pathology Core Staff. Briefly, tissues were fixed with 4% formaldehyde and embedded in paraffin. Sections after the removal of paraffin were stained with hematoxylin and eosin. Lipid droplet size and number of nuclei were quantified by using MetaMorph software. Mice were injected intraperitoneally

with CL316243 (0.1 mg/kg) or PBS and killed at 10 min after injection to collect fat tissues.

Quantitative RT–PCR (RT–qPCR) and detection of *Ucp1* 3′-UTRs

Total RNA was extracted by using TOOLSmart RNA Extractor following the manufacturer's protocol (TOOLS Biotech). Total RNA and RNA from sucrose gradient fractions and immunoprecipitated complexes were reverse-transcribed by using random primers and ImProm-II reverse transcriptase (Promega). The synthesized cDNAs were analyzed by qPCR with the Universal Probe Library or SYBR Green reagents in the LightCycler 480 system (Roche). The relative expression of designated targets was calculated by the comparative threshold cycle value with *Gapdh* mRNA as the reference. For absolute qPCR quantification of *Ucp1* and *Cpeb2* mRNAs in human (purchased from iBiologics) and mouse BAT, the cDNA reaction (reverse-transcribed from 0.01 μg total RNA) was used for 10 μl qPCR. The concentration of standard DNA template in the qPCR ranged from ~7 pM to ~0.2 fM. The quantification of all four *Cpeb* mRNAs in mouse BAT and HIB1B adipocytes was also performed similarly. To amplify *Ucp1* 3′-UTRs, total RNA from human and mouse BAT was reverse-transcribed by using VdT-linker primer, followed by PCR with dT6-linker and a human- or mouse-specific sense primer. The primer sequences are in Appendix Table S1.

Polysome profile analysis and RNA immunoprecipitation (RNA-IP)

Brown adipose tissue was lysed in polysome buffer (25 mM Hepes, pH 7.5, 25 mM NaCl, 5 mM $MgCl_2$, 0.3% NP-40, 100 μg/ml cycloheximide, 0.5 mM DTT, 20 U/ml RNase inhibitor, and 1X protease inhibitor cocktail) and centrifuged at 15,000 × *g* for 15 min at 4°C. The supernatant was layered on top of a linear 15–50% (w/v) sucrose gradient and then centrifuged in a SW41 rotor at 170,000 × *g* for 2 h. Polysome profiles were monitored by 254 nm absorbance with the ISCO density gradient system. For RNA-IP, BAT was lysed in IP buffer (50 mM Hepes, pH 7.4, 150 mM NaCl, 1 mM $MgCl_2$, 0.5% Triton X-100, 10% glycerol, 1 mM DTT, 1X protease inhibitor cocktail, and RNase inhibitor) and centrifuged at 15,000 × *g* for 15 min. The supernatant was divided and incubated with protein G beads bound with CPEB2 or control IgG for 3 h. The precipitated substances were immunoblotted with CPEB2 or eluted with the buffer containing 100 mM Tris, pH 8, 10 mM EDTA, and 1% SDS. The latter samples as well as gradient fractions were treated with 100 μg/ml Proteinase K for 30 min at 37°C, phenol/chloroform-extracted, and ethanol-precipitated to obtain RNA for RT–qPCR.

Poly(A) tail (PAT) assay

The length of the poly(A) tail of mRNAs was determined by the use of a poly(A) tail-length assay kit (Affymetrix) as the manufacturer instructed. Briefly, the first 3′-end G/I tailing reaction permitted subsequent cDNA synthesis from the end of mRNAs with the primer 5′-CCCCCCTT-3′. The following PCR involved the gene-specific forward primer (mUcp1L or mUcp1F) located upstream of poly(A), and the 5′-CCCCCCTT-3′ reverse primer and the PCR products were analyzed on 2% agarose gels. To remove the poly(A) tail before PAT assay, 3 μg total RNA from BAT was annealed with 100 pmol oligo(dT) primer, digested with RNaseH at 37°C for 20 min, and then treated with DNase for another 15 min. The free nucleotides in the reactions were removed by using a DyeEx spin column (Qiagen), and the flow through was phenol/chloroform-extracted and ethanol-precipitated. Approximately 0.2 μg total RNA was used for subsequent PAT assay. The mUcp1L and mUcp1F primer sequences are in Appendix Table S1.

BAT temperature measurement

To measure BAT temperature in ambulatory mice, mice under 1.2% Avertin-induced anesthesia were shaved ~2 cm below the head, and the TA-F10 temperature probe (DSI, Harvard Bioscience) was implanted onto the interscapular BAT pad in a shallow incision. After 1-week recovery, BAT temperature was measured by using DSI telemetric transmitters. The data were recorded every minute for 2 days and then averaged to obtain mean BAT temperature during 12-h light time for each mouse. For pharmacological experiments, the data were recorded every minute for 15 min and 2 h before and after CL316243 injection and then averaged in 5-min intervals for each mouse.

Recombinant adeno-associated virus (AAV) production and AAV administration in BAT

The DNA fragment containing the myc-tagged C-terminus of CPEB2 was excised with NheI and PmeI from pcDNA3.1-myc-CPEB2RBD (Chen & Huang, 2012) and then cloned into the XbaI-HincII-digested pAAV-MCS vector. The AAV-CPEB2 plasmid was previously generated (Lu *et al*, 2017). Along with the pHelper and AAV2/8 plasmids, the plasmid mixture was delivered to human embryonic kidney 293 (HEK293) cells by calcium phosphate transfection. The recombinant AAV viruses were purified by two rounds of cesium chloride sedimentation, and titers were assessed by qPCR as described (Chen *et al*, 2009). The mice receiving AAV were under the same surgical procedures described for implanting the TA-F10 temperature probe. Approximately 2×10^{10} vg (vector genome) recombinant AAV in 30 μl PBS was injected triangularly into interscapular BAT (10 μl per site).

^{18}F-fluorodeoxyglucose positron emission tomography (^{18}FDG-PET) scanning

^{18}FDG-PET scanning in mice was conducted with blinding to genotypes by the Taiwan Mouse Clinic staff. Briefly, mice with free access to water fasted overnight. Mice intravenously injected with 0.45 mCi of ^{18}F-FDG radiotracer rested for 1 h before 30-min scanning by the use of the microPET R4 system (Concorde Microsystems, Siemens). For cold exposure study, mice were placed at 4°C for 4 h and another 1 h after ^{18}F-FDG injection and then underwent PET imaging.

Energy expenditure measurements by indirect calorimetry

Metabolic rates were measured by Oxymax/CLAMS indirect calorimetry (Columbus Instruments), operated by the Taiwan Mouse Clinic staff without knowing mouse genotypes. The energy

expenditure (i.e., heat production) was calculated by measuring oxygen consumption and carbon dioxide production according to the built-in formula (Even & Nadkarni, 2012; Nie *et al*, 2015). Mice were housed in individual cages with constant temperature (22°C) and humidity over 12:12 light/dark cycles with *ad libitum* access to food and water. After 64-h acclimatization to the new environment, mice were recorded for 98 h at different temperatures or in response to intraperitoneal injection of CL316243 (0.2 mg/kg). The maximal capacity in our system allows for consecutive monitoring of 16 metabolic cages and two reference chambers for 1 min per cage at a time, so metabolic data in each mouse were collected every 18 min. Energy expenditure at 22, 30, and 4°C was average data obtained from 12-, 10-, and 4-h recordings, respectively. CL316243-promoted energy expenditure is presented as mean values from every 126-min recording.

Cell culture and luciferase reporter assay

Mouse HIB1B cells were grown in DMEM with 10% fetal bovine serum. For adipocyte differentiation, cells were cultured to confluence, incubated in fresh medium containing 0.5 μM dexamethasone, 0.5 mM 3-isobutyl-1-methylxanthine, 20 nM insulin, and 1 nM triiodothyronine (T3) for 2 days, and then switched to 20 nM insulin and 1 nM T3 for another week. Differentiated cells were transfected with the plasmids expressing Rluc, Fluc appended with *mUcp1*- or *hUcp1*-3'UTR, and full-length or truncated CPEB2 by TurboFect transfection reagent for 3 h, which was replaced with new medium for 24 h, and then treated with ±10 μM CL316243 for 12 h before harvesting for dual luciferase reporter assay (Promega) and RT–qPCR to detect normalized Fluc/Rluc RNA level.

Western blot analysis

Tissues were homogenized on ice in the lysis buffer containing 20 mM Hepes, pH 7.5, 250 mM sucrose, 10 mM KCl, 1.5 mM $MgCl_2$, 1 mM EDTA, 0.5% sodium deoxycholate, 0.1% SDS, 1% Triton X-100, and 1X protease inhibitor cocktail mix (Roche), and then centrifuged at 15,000 × *g* for 15 min at 4°C. The protein concentration of collected supernatants was determined by the use of Pierce BCA Protein Assay Kit. Samples with equal amount of protein were denatured at 95°C for 5 min, separated on a 10% SDS–PAGE, and then transferred to polyvinylidene fluoride (PVDF) membrane (Millpore), which was incubated with the primary antibodies followed by horseradish peroxidase-conjugated secondary antibodies (Appendix Table S2) and detection with chemiluminescence substrates. All uncropped immunoblot images are shown in Appendix Fig S4.

Immunofluorescence staining

Unless otherwise specified, all procedures were performed at room temperature with three washes of PBS between changes of reagents. Fixed BAT sections after paraffin removal were immersed in 0.1% Sudan Black B in 70% ethanol for 20 min to quench autofluorescence (Viegas *et al*, 2007). After three washes of PBST (0.02% Tween-20 in PBS), sections were permeabilized with 0.2% Triton X-100 in PBS, blocked in 10% horse serum for 1 h, and then incubated with primary antibodies (Appendix Table S2) at 4°C overnight. After 1-h incubation of fluorophore-conjugated secondary antibodies (Appendix Table S2) and Hoechst 33342, slices were washed with PBS three times before mounting with ProLong Gold Antifade Reagent (Invitrogen). Fluorescence images were acquired under a LSM700META confocal microscope (Carl Zeiss).

Plasmid construction

Ucp1 3′-UTR was PCR-amplified from human or mouse BAT cDNA using the primers, 5′-TGCTCTAGATCAGCTTCAAGAAAATGATG TA-3′ and 5′-ACGCGTC GACAAAAGGTATTAGCAATACTTTAT-3′ (human); the sense primer 5′-TGCTCT AGAGCAACTTGGAGGAA GAGAT-3′ with 5′-ACGCGTCGACAGATGGAATTAG CAATACTTTA-3′ and 5′-ACGCGTCGACGATTTCTTTGGTTGGTTTTAT-3′ for long and short forms, respectively. The XbaI-SalI-digested DNA fragments were cloned into the pGL3-promoter vector (Promega). To create Fluc-*mUcp1LΔHex* Fluc-*mUcp1LmutCPE* and Fluc-*hUcp1SNP1 + 2* reporters, the QuikChange II site-directed mutagenesis kit (Stratagene) and the sense and antisense primers, ΔHex, 5′-GTTCACAGCTAATATACT CAACGGAGTATTGCTAATTCCATCT-3′ and 5′-AG ATGGAATTAGC AATACTCCGTTGAGTATATTAGCTGTGAAC-3′; CPEmut1, 5′-G AGT TTTGAAACCTCTTTTGGCTTTTTTTAAAGGGAAAACTAAC-3′ and 5′-G TTAGTTTTCCCTTTAAAAAAAGCCAAAAGAGGTTTCAAAACTC-3′; CPEmut2, 5′-TAACACATACACATAGTTTTGCCTCTTACTGTCT TAAAGACA-3′ and 5′-TGTCTTTAAGACAGTAAGAGGCAAAACTATG TGTATGTGTTA-3′; SNP1 5′-TGAAGTTATTAAAAATATTAGTCTT TATTAACCACAGTTGTC-3′ and 5′-GA CAACTGTGGTTAATAAA GACTAATATTTTTAATAACTTCA-3′; SNP2 5′-CAGA GAATTTTGGA CTTTTTTGTATAAAAAAGAGGAAAATTAATG-3′ and 5′-CATT AAT TTTCCTCTTTTTTATACAAAAAAGTCCAAAATTCTCTG-3′, were used.

Northern blot analysis

Brown adipose tissue total RNA (5 μg) was separated on a 1% agarose/2% formaldehyde gel in 1X MOPS buffer (20 mM MOPS, pH 7, 5 mM NaOAc, 1 mM EDTA) and transferred to GeneScreen Plus hybridization transfer membrane (PerkinElmer). Radiolabeled DNA probes were prepared by hexamer random priming in the presence of [α-^{32}P]-dCTP. The primers used to amplify DNA templates for probe synthesis were for mouse UCP1, 5′-GCCAGGATGGT GAACCCGA-3′ and 5′-TTATGTGGTACAATCCACTGTC-3′; human UCP1, 5′-AAGATGGGGGGCCTGACAG-3′ and 5′-TGTGGCACAGTC CATAGTCT-3′; and 18S rRNA, 5′-TGAAATTCTTGGACCGGCGC-3′ and 5′-GGGCCTCACTAAACCATCCA-3′. Radioactive products were visualized and quantified with a phosphoimager.

Data presentation and statistical analysis

Data are mean ± SD ($n < 5$) or mean ± SEM ($n >= 5$) specified in figure legends. Statistical analyses involved the use of GraphPad Prism software with the recommended methods for assessing normality (Shapiro–Wilk test) and variances (Brown–Forsythe test) and *post hoc* comparing statistical differences between groups (Tukey's multiple comparison). Most data compared by Student's *t*-test passed Shapiro–Wilk normality test except those in Fig 4E droplet size (12 mo WT data) and Fig 4F BAT weight (12 mo, KO

data). Sample sizes and statistical methods (ANOVA or two-tailed unpaired Student's *t*-test unless otherwise specified) for experiments are in figure legends. Pearson's correlation coefficient was calculated to evaluate the correlated expression between *Ucp1* mRNA and other designated mRNA levels.

Expanded View for this article is available online.

Acknowledgements
We appreciate Bruce Spiegelman for HIB1B cells, Heng Lin for pHelper and AAV2/8 plasmids, Cheng-Pu Sun and Mi-Hua Tao for HEK293 cells and technical assistance in AAV packaging, and Po-Jen Chen for CPEB2 antibody generation. We thank the Taiwan Mouse Clinic (TMC), which is funded by MoST (106-2319-B-001-004), for PET scan experiments, the pathology core for tissue processing, and the transgenic core for blastocyst microinjection. This work was supported by the National Health Research Institute (NHRI-EX104-10437SI) and Ministry of Science and Technology of Taiwan (MoST105-2311-B-001-078-MY3). HFC was supported by a postdoctoral fellowship (2013–2014) from Academia Sinica.

Author contributions
H-FC designed and conducted and performed the experiments, analyzed the data, and wrote the manuscript. C-MH maintained animals and produced AAV virus. Y-SH designed and supervised the study, co-wrote the manuscript, and is responsible for its content.

Conflict of interest
The authors declare that they have no conflict of interest.

References

Balogh AG, Ridley RG, Patel HV, Freeman KB (1989) Rabbit brown adipose tissue uncoupling protein MRNA: use of only one of two polyadenylation signals in its processing. *Biochem Biophys Res Commun* 161: 156 – 161

Barrett LW, Fletcher S, Wilton SD (2012) Regulation of eukaryotic gene expression by the untranslated gene regions and other non-coding elements. *Cell Mol Life Sci* 69: 3613 – 3634

Basu S, Hess S, Nielsen Braad PE, Olsen BB, Inglev S, Hoilund-Carlsen PF (2014) The basic principles of FDG-PET/CT imaging. *PET Clin* 9: 355 – 370

Bava FA, Eliscovich C, Ferreira PG, Minana B, Ben-Dov C, Guigo R, Valcarcel J, Mendez R (2013) CPEB1 coordinates alternative 3′-UTR formation with translational regulation. *Nature* 495: 121 – 125

Bouillaud F, Ricquier D, Thibault J, Weissenbach J (1985) Molecular approach to thermogenesis in brown adipose tissue: cDNA cloning of the mitochondrial uncoupling protein. *Proc Natl Acad Sci USA* 82: 445 – 448

Cannon B, Houstek J, Nedergaard J (1998) Brown adipose tissue. More than an effector of thermogenesis? *Ann N Y Acad Sci* 856: 171 – 187

Cannon B, Nedergaard J (2011) Nonshivering thermogenesis and its adequate measurement in metabolic studies. *J Exp Biol* 214: 242 – 253

Carter EA, Bonab AA, Paul K, Yerxa J, Tompkins RG, Fischman AJ (2011) Association of heat production with 18F-FDG accumulation in murine brown adipose tissue after stress. *J Nucl Med* 52: 1616 – 1620

Chao HW, Lai YT, Lu YL, Lin CL, Mai W, Huang YS (2012) NMDAR signaling facilitates the IPO5-mediated nuclear import of CPEB3. *Nucleic Acids Res* 40: 8484 – 8498

Chao HW, Tsai LY, Lu YL, Lin PY, Huang WH, Chou HJ, Lu WH, Lin HC, Lee PT, Huang YS (2013) Deletion of CPEB3 enhances hippocampus-dependent memory via increasing expressions of PSD95 and NMDA receptors. *J Neurosci* 33: 17008 – 17022

Chechi K, Carpentier AC, Richard D (2013) Understanding the brown adipocyte as a contributor to energy homeostasis. *Trends Endocrinol Metab* 24: 408 – 420

Chen CC, Sun CP, Ma HI, Fang CC, Wu PY, Xiao X, Tao MH (2009) Comparative study of anti-hepatitis B virus RNA interference by double-stranded adeno-associated virus serotypes 7, 8, and 9. *Mol Ther* 17: 352 – 359

Chen PJ, Huang YS (2012) CPEB2-eEF2 interaction impedes HIF-1alpha RNA translation. *EMBO J* 31: 959 – 971

Conway AE, Van Nostrand EL, Pratt GA, Aigner S, Wilbert ML, Sundararaman B, Freese P, Lambert NJ, Sathe S, Liang TY, Essex A, Landais S, Burge CB, Jones DL, Yeo GW (2016) Enhanced CLIP uncovers IMP protein-RNA targets in human pluripotent stem cells important for cell adhesion and survival. *Cell Rep* 15: 666 – 679

Dai N, Zhao L, Wrighting D, Kramer D, Majithia A, Wang Y, Cracan V, Borges-Rivera D, Mootha VK, Nahrendorf M, Thorburn DR, Minichiello L, Altshuler D, Avruch J (2015) IGF2BP2/IMP2-Deficient mice resist obesity through enhanced translation of Ucp1 mRNA and other mRNAs encoding mitochondrial proteins. *Cell Metab* 21: 609 – 621

Dulloo AG (2013) Translational issues in targeting brown adipose tissue thermogenesis for human obesity management. *Ann N Y Acad Sci* 1302: 1 – 10

Enerback S, Jacobsson A, Simpson EM, Guerra C, Yamashita H, Harper ME, Kozak LP (1997) Mice lacking mitochondrial uncoupling protein are cold-sensitive but not obese. *Nature* 387: 90 – 94

Even PC, Nadkarni NA (2012) Indirect calorimetry in laboratory mice and rats: principles, practical considerations, interpretation and perspectives. *Am J Physiol Regul Integr Comp Physiol* 303: R459 – R476

Feldmann HM, Golozoubova V, Cannon B, Nedergaard J (2009) UCP1 ablation induces obesity and abolishes diet-induced thermogenesis in mice exempt from thermal stress by living at thermoneutrality. *Cell Metab* 9: 203 – 209

Gaudry MJ, Jastroch M, Treberg JR, Hofreiter M, Paijmans JLA, Starrett J, Wales N, Signore AV, Springer MS, Campbell KL (2017) Inactivation of thermogenic UCP1 as a historical contingency in multiple placental mammal clades. *Sci Adv* 3: e1602878

Gerhart-Hines Z, Feng D, Emmett MJ, Everett LJ, Loro E, Briggs ER, Bugge A, Hou C, Ferrara C, Seale P, Pryma DA, Khurana TS, Lazar MA (2013) The nuclear receptor Rev-erbalpha controls circadian thermogenic plasticity. *Nature* 503: 410 – 413

Golozoubova V, Hohtola E, Matthias A, Jacobsson A, Cannon B, Nedergaard J (2001) Only UCP1 can mediate adaptive nonshivering thermogenesis in the cold. *FASEB J* 15: 2048 – 2050

Golozoubova V, Cannon B, Nedergaard J (2006) UCP1 is essential for adaptive adrenergic nonshivering thermogenesis. *Am J Physiol Endocrinol Metab* 291: E350 – E357

Hagele S, Kuhn U, Boning M, Katschinski DM (2009) Cytoplasmic polyadenylation-element-binding protein (CPEB)1 and 2 bind to the HIF-1alpha mRNA 3′-UTR and modulate HIF-1alpha protein expression. *Biochem J* 417: 235 – 246

Hake LE, Richter JD (1994) CPEB is a specificity factor that mediates cytoplasmic polyadenylation during *Xenopus* oocyte maturation. *Cell* 79: 617 – 627

Hankir MK, Kranz M, Keipert S, Weiner J, Andreasen SG, Kern M, Patt M, Kloting N, Heiker JT, Brust P, Hesse S, Jastroch M, Fenske WK (2017) Dissociation between brown adipose tissue (18)F-FDG uptake and thermogenesis in uncoupling protein 1-deficient mice. *J Nucl Med* 58: 1100 – 1103

Hu W, Yuan B, Lodish HF (2014) Cpeb4-mediated translational regulatory circuitry controls terminal erythroid differentiation. *Dev Cell* 30: 660 – 672

Huang YS, Kan MC, Lin CL, Richter JD (2006) CPEB3 and CPEB4 in neurons: analysis of RNA-binding specificity and translational control of AMPA receptor GluR2 mRNA. *EMBO J* 25: 4865 – 4876

Igea A, Mendez R (2010) Meiosis requires a translational positive loop where CPEB1 ensues its replacement by CPEB4. *EMBO J* 29: 2182 – 2193

Inokuma K, Ogura-Okamatsu Y, Toda C, Kimura K, Yamashita H, Saito M (2005) Uncoupling protein 1 is necessary for norepinephrine-induced glucose utilization in brown adipose tissue. *Diabetes* 54: 1385 – 1391

Ivshina M, Lasko P, Richter JD (2014) Cytoplasmic polyadenylation element binding proteins in development, health, and disease. *Annu Rev Cell Dev Biol* 30: 393 – 415

Kan MC, Oruganty-Das A, Cooper-Morgan A, Jin G, Swanger SA, Bassell GJ, Florman H, van Leyen K, Richter JD (2010) CPEB4 is a cell survival protein retained in the nucleus upon ischemia or endoplasmic reticulum calcium depletion. *Mol Cell Biol* 30: 5658 – 5671

Kontani Y, Wang Y, Kimura K, Inokuma KI, Saito M, Suzuki-Miura T, Wang Z, Sato Y, Mori N, Yamashita H (2005) UCP1 deficiency increases susceptibility to diet-induced obesity with age. *Aging Cell* 4: 147 – 155

Lai YT, Su CK, Jiang ST, Chang YJ, Lai AC, Huang YS (2016) Deficiency of CPEB2-confined choline acetyltransferase expression in the dorsal motor nucleus of vagus causes hyperactivated parasympathetic signaling-associated bronchoconstriction. *J Neurosci* 36: 12661 – 12676

Lateef DM, Abreu-Vieira G, Xiao C, Reitman ML (2014) Regulation of body temperature and brown adipose tissue thermogenesis by bombesin receptor subtype-3. *Am J Physiol Endocrinol Metab* 306: E681 – E687

Liew CW, Boucher J, Cheong JK, Vernochet C, Koh HJ, Mallol C, Townsend K, Langin D, Kawamori D, Hu J, Tseng YH, Hellerstein MK, Farmer SR, Goodyear L, Doria A, Bluher M, Hsu SI, Kulkarni RN (2013) Ablation of TRIP-Br 2, a regulator of fat lipolysis, thermogenesis and oxidative metabolism, prevents diet-induced obesity and insulin resistance. *Nat Med* 19: 217 – 226

Lin CL, Evans V, Shen S, Xing Y, Richter JD (2010) The nuclear experience of CPEB: implications for RNA processing and translational control. *RNA* 16: 338 – 348

Liu M, Bai J, He S, Villarreal R, Hu D, Zhang C, Yang X, Liang H, Slaga TJ, Yu Y, Zhou Z, Blenis J, Scherer PE, Dong LQ, Liu F (2014) Grb10 promotes lipolysis and thermogenesis by phosphorylation-dependent feedback inhibition of mTORC1. *Cell Metab* 19: 967 – 980

Lowell BB, S-Susulic V, Hamann A, Lawitts JA, Himms-Hagen J, Boyer BB, Kozak LP, Flier JS (1993) Development of obesity in transgenic mice after genetic ablation of brown adipose tissue. *Nature* 366: 740 – 742

Lowell BB, Spiegelman BM (2000) Towards a molecular understanding of adaptive thermogenesis. *Nature* 404: 652 – 660

Lu WH, Yeh NH, Huang YS (2017) CPEB2 activates GRASP1 mRNA translation and promotes AMPA receptor surface expression, long-term potentiation, and memory. *Cell Rep* 21: 1783 – 1794

van Marken Lichtenbelt WD, Vanhommerig JW, Smulders NM, Drossaerts JM, Kemerink GJ, Bouvy ND, Schrauwen P, Teule GJ (2009) Cold-activated brown adipose tissue in healthy men. *N Engl J Med* 360: 1500 – 1508

Mendez R, Murthy KG, Ryan K, Manley JL, Richter JD (2000) Phosphorylation of CPEB by Eg2 mediates the recruitment of CPSF into an active cytoplasmic polyadenylation complex. *Mol Cell* 6: 1253 – 1259

Moore MJ (2005) From birth to death: the complex lives of eukaryotic mRNAs. *Science* 309: 1514 – 1518

Morrison SF, Madden CJ, Tupone D (2014) Central neural regulation of brown adipose tissue thermogenesis and energy expenditure. *Cell Metab* 19: 741 – 756

Nedergaard J, Golozoubova V, Matthias A, Asadi A, Jacobsson A, Cannon B (2001) UCP1: the only protein able to mediate adaptive non-shivering thermogenesis and metabolic inefficiency. *Biochim Biophys Acta* 1504: 82 – 106

Nie Y, Gavin TP, Kuang S (2015) Measurement of resting energy metabolism in mice using oxymax open circuit indirect calorimeter. *Bio Protoc* 5: e1602

O'Neill SM, Hinkle C, Chen SJ, Sandhu A, Hovhannisyan R, Stephan S, Lagor WR, Ahima RS, Johnston JC, Reilly MP (2014) Targeting adipose tissue via systemic gene therapy. *Gene Ther* 21: 653 – 661

Ortiz-Zapater E, Pineda D, Martinez-Bosch N, Fernandez-Miranda G, Iglesias M, Alameda F, Moreno M, Eliscovich C, Eyras E, Real FX, Mendez R, Navarro P (2011) Key contribution of CPEB4-mediated translational control to cancer progression. *Nat Med* 18: 83 – 90

Park A, Kim WK, Bae KH (2014) Distinction of white, beige and brown adipocytes derived from mesenchymal stem cells. *World J Stem Cells* 6: 33 – 42

Pavlopoulos E, Trifilieff P, Chevaleyre V, Fioriti L, Zairis S, Pagano A, Malleret G, Kandel ER (2011) Neuralized1 activates CPEB3: a function for nonproteolytic ubiquitin in synaptic plasticity and memory storage. *Cell* 147: 1369 – 1383

Peng SC, Lai YT, Huang HY, Huang HD, Huang YS (2010) A novel role of CPEB3 in regulating EGFR gene transcription via association with Stat5b in neurons. *Nucleic Acids Res* 38: 7446 – 7457

Porter C, Herndon DN, Chondronikola M, Chao T, Annamalai P, Bhattarai N, Saraf MK, Capek KD, Reidy PT, Daquinag AC, Kolonin MG, Rasmussen BB, Borsheim E, Toliver-Kinsky T, Sidossis LS (2016) Human and mouse brown adipose tissue mitochondria have comparable UCP1 function. *Cell Metab* 24: 246 – 255

Puigserver P, Wu Z, Park CW, Graves R, Wright M, Spiegelman BM (1998) A cold-inducible coactivator of nuclear receptors linked to adaptive thermogenesis. *Cell* 92: 829 – 839

Rial E, Gonzalez-Barroso MM (2001) Physiological regulation of the transport activity in the uncoupling proteins UCP1 and UCP2. *Biochim Biophys Acta* 1504: 70 – 81

Ross SR, Choy L, Graves RA, Fox N, Solevjeva V, Klaus S, Ricquier D, Spiegelman BM (1992) Hibernoma formation in transgenic mice and isolation of a brown adipocyte cell line expressing the uncoupling protein gene. *Proc Natl Acad Sci USA* 89: 7561 – 7565

Stebbins-Boaz B, Cao Q, de Moor CH, Mendez R, Richter JD (1999) Maskin is a CPEB-associated factor that transiently interacts with eIF-4E. *Mol Cell* 4: 1017 – 1027

Takahashi A, Adachi S, Morita M, Tokumasu M, Natsume T, Suzuki T, Yamamoto T (2015) Post-transcriptional stabilization of Ucp1 mRNA protects mice from diet-induced obesity. *Cell Rep* 13: 2756 – 2767

Tian B, Manley JL (2017) Alternative polyadenylation of mRNA precursors. *Nat Rev Mol Cell Biol* 18: 18 – 30

Tomilov A, Bettaieb A, Kim K, Sahdeo S, Tomilova N, Lam A, Hagopian K, Connell M, Fong J, Rowland D, Griffey S, Ramsey J, Haj F, Cortopassi G (2014) Shc depletion stimulates brown fat activity *in vivo* and *in vitro*. *Aging Cell* 13: 1049 – 1058

Tsai LY, Chang YW, Lin PY, Chou HJ, Liu TJ, Lee PT, Huang WH, Tsou YL, Huang YS (2013) CPEB4 knockout mice exhibit normal hippocampus-related synaptic plasticity and memory. *PLoS One* 8: e84978

Viegas MS, Martins TC, Seco F, do Carmo A (2007) An improved and cost-effective methodology for the reduction of autofluorescence in direct immunofluorescence studies on formalin-fixed paraffin-embedded tissues. *Eur J Histochem* 51: 59 – 66

Wang W, Seale P (2016) Control of brown and beige fat development. *Nat Rev Mol Cell Biol* 17: 691 – 702

Whittle AJ, Carobbio S, Martins L, Slawik M, Hondares E, Vazquez MJ, Morgan D, Csikasz RI, Gallego R, Rodriguez-Cuenca S, Dale M, Virtue S, Villarroya F, Cannon B, Rahmouni K, Lopez M, Vidal-Puig A (2012) BMP8B increases brown adipose tissue thermogenesis through both central and peripheral actions. *Cell* 149: 871 – 885